SUPPLEMENT TO THE *WELDING JOURNAL*, FEBRUARY 2012
Sponsored by the American Welding Society and the Welding Research Council

Partial Transient Liquid Phase Diffusion Brazing of Copper-Beryllium Alloy (C17200) Using Silver-Based Interlayer

Microstructural and hardness differences were characterized for three silver-based filler metals

BY M. MAZAR ATABAKI

ABSTRACT

Partial transient liquid phase diffusion brazing was employed to join copper-beryllium alloy using three silver-based interlayers. The brazing process was carried out at different temperatures under argon and vacuum atmospheres for various hold times. Interfacial microstructures were examined by scanning electron microscopy and energy dispersive spectroscopy elemental analyses. Microhardness, tensile, and fatigue tests were used to evaluate the mechanical properties. A maximum tensile strength of 156.45 MPa was obtained for joints processed at 780°C. Fatigue strength of joints fabricated in vacuum was higher than those of joints prepared in argon atmosphere. Brittle phases were formed in the brazed region, and the joint strength and toughness were dramatically decreased, especially in the specimens brazed with Cd-containing interlayers. The study indicates the existence of $CdCu_2$ (β_x), $CdCu_4$ (β_y), Ag_5Zn_8, CuZn (β'), Cu_3Sn, and Ag_3Sn in the fusion zone. The alloying elements were considerably diffused from the interlayers into the alloy grain boundaries.

Introduction

Copper-beryllium alloys are preferred in critical applications ranging from miniature electronic connectors to aircraft bushings to oil field drill tooling applications, as well as plastic and die cast mold tooling and nonsparking hand tools (Ref. 1). Among the various types of copper-beryllium alloys, precipitated-hardening copper-beryllium alloy (C17200) is widely used in different springs due to its low elastic module and high strength. This alloy is being solution annealed to increase its formability and precipitation hardened (age hardened) to improve the strength. The alloy usually contains a third element (cobalt or nickel) to produce solid solution and dispersion beryllide particles in the matrix (Ref. 2). The solution-annealed and age-hardened alloy suffers a serious and irreversible loss of mechanical properties when welded. Welded joints in the alloy must, therefore, be designed to take account of this loss. A limited amount of welding is carried out on the heat-treatable alloy. To avoid cracking of the hardened material during welding, and to facilitate subsequent heat treatment, welding was normally carried out in the solution-treated condition, followed by a reheat treatment to regain some of the properties of the hardened material. The copper, beryllium alloy forms refractory oxides that rarely can be dispersed by the fusion welding processes. Another risk involved in using such a technique is that solidification of the nonmatching weld metal will occur before solidification of the base metal, possibly causing heat-affected zone cracking and incurring the danger of differential corrosion between the base and filler metals in service (Ref. 3). Many of the problems of welded joints for the alloy can be overcome by partial transient liquid phase diffusion metallic brazing (Ref. 4). This brazing technique exploits thin metallic films that melt at relatively low temperatures as part of a multimaterial interlayer to enable joining at reduced temperatures (Refs. 5, 6). Partial transient liquid phase diffusion brazing is a modified version of transient liquid phase brazing, which is usually used for joining of ceramics (Refs. 7–9). During this process, only a limited portion of interlayer melts and then reacts with the base metal. Recently, this technique was used to join dissimilar metals in critical applications like nuclear power plants (Refs. 10, 11). For a given operating temperature, the joining method relies on the time required to prevent the formation of brittle phases.

One of the vital aspects for the brazing process is the selection of the interlayer. The interlayer design including its composition and thickness determines the final behavior of the joints. In addition, joining of the high-strength alloy with a high melting point filler metal negatively influences the joining substrate. This parameter directly affects the brazing time, which is necessary to prevent the formation of nonequilibrium solidification products that form during cooling and degrade material properties. For this purpose, Ag-based interlayers are perfect candidates to join copper-beryllium alloys. Compared to Cu- and Ni-based interlayers, Ag-based interlayers have the advantage of a relatively low brazing temperature. Furthermore, addition of small quantities of Sn in the interlayer increases its wettability due to diffusion of Sn across the interface, and addition of Cd

M. MAZAR ATABAKI (pmmmaa@leeds.ac.uk) *is with Institute for Materials Research, the School of Process, Environmental, and Materials Engineering, Faculty of Engineering, University of Leeds, Leeds, UK; and Department of Mechanical Engineering, Faculty of Materials Engineering, University of Technology Malaysia, Malaysia.*

KEYWORDS

Copper-Beryllium
Transient Liquid Phase
Diffusion Bonding
Microstructure
Intermetallics

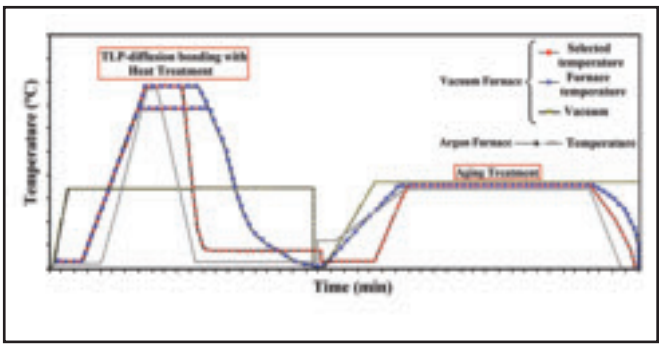

Fig. 1 — Cycle of transient liquid phase diffusion brazing of the copper-beryllium alloy.

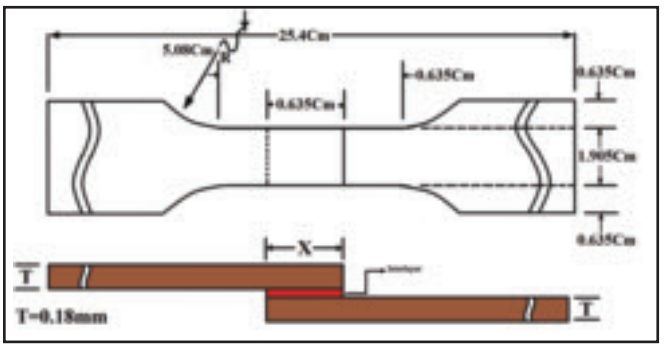

Fig. 2 — Schematic diagram of tensile and fatigue specimens.

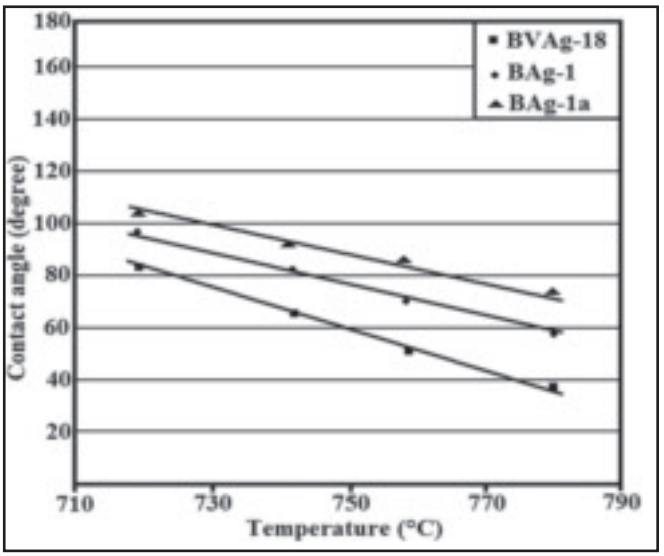

Fig. 3 — Variation of contact angle with temperature for three different interlayers.

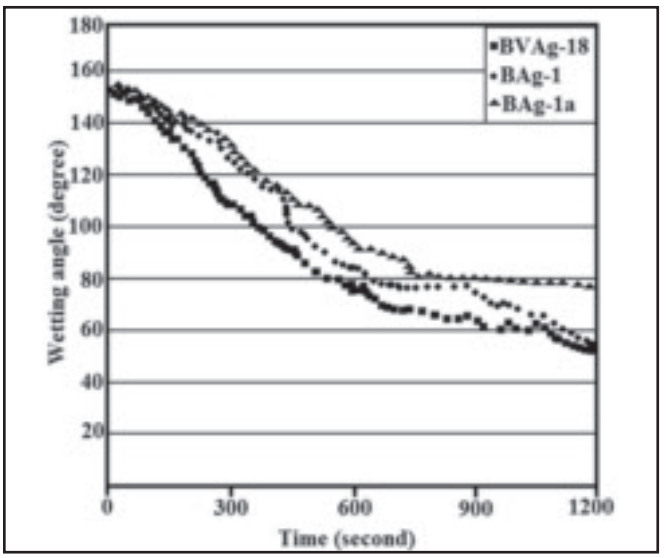

Fig 4 — The sessile drop tests of the interlayers on the copper-beryllium substrate at 780°C for 0–1200 s.

reduces the solidus temperature and melting range and improves the fluidity of the Ag-based interlayer. These low-vapor pressure interlayers meet the need for a composition free from volatile constituents, particularly essential in the joining of the special alloy. There is some propensity for the insert metal to liquate, but this is minimized by rapid heating to the brazing temperature. It is also important to consider any heat treatments that may be required for the base metal, because the brazed specimens must withstand the temperature involved. The Ag-based interlayers have a low interaction rate with the alloy and offer good oxidation resistance. Among the various types of Ag-based interlayers, BAg-1, BAg-1a, and BVAg-18 have the abovementioned properties. These interlayers are compositionally more uniform than the other ones even after crystallization during the brazing operation when a fine mixture of phases is formed. Such homogenized mixture melts over a narrower temperature range under transient heating. This is an outcome of shorter distances over which atoms of different elements in different phases have to diffuse in order to form a uniform liquid phase. The interlayers are also well compatible with the base metal.

In the present study, the partial transient liquid phase diffusion brazing method was used to join a copper-beryllium alloy with different Ag-based filler metals. Microstructural and compositional changes were characterized, and hardness was measured in different bond regions. The analysis was coupled with the strength and fatigue measurements of the specimens. The differences in the microstruc-

Table 1 — Chemical Composition of the Copper-Beryllium Alloy

	Chemical Composition (wt-%)				
Alloy	Cu	Be	Ni	Co	Pb
C17200	Bal.	1.92	0.50	0.10	0.10

Table 2 — Chemical Composition of the Interlayers

	Chemical Composition (%-wt)				
Interlayer	Ag	Cu	Zn	Cd	Sn
BV Ag-18	54	32	—	—	14
BAg-1	44.5	15	16	24.5	—
BAg-1a	51.562	15	16	17.438	—

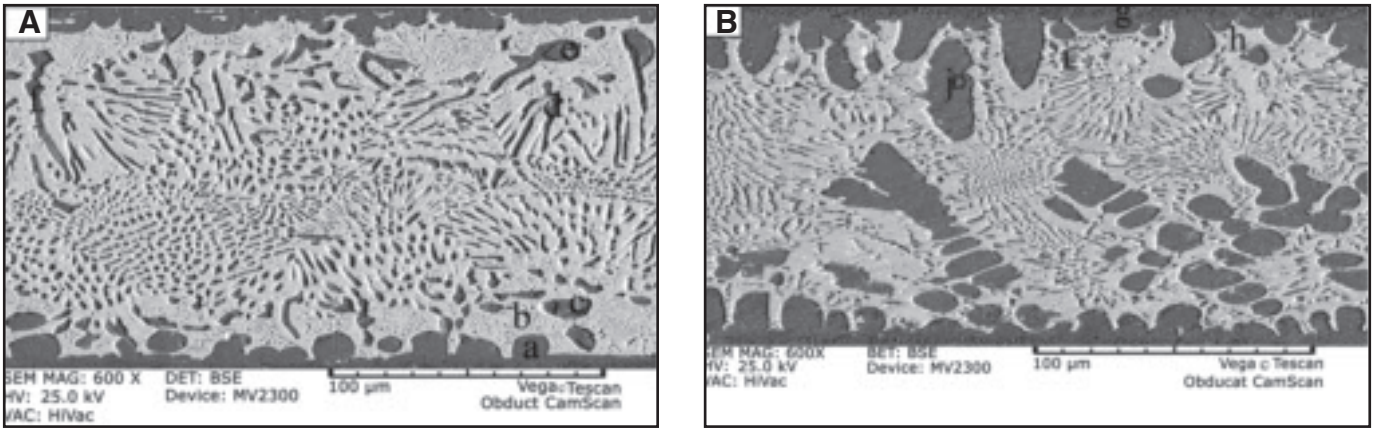

Fig. 5 — SEM microstructure of the copper-beryllium alloy brazed at 780°C for 20 min. A — BAg-1a; B — BAg-1; C — BVAg-18.

ture of the bonds with three different interlayers are comprehensively discussed with existed modeling output and direct microstructural observation.

Experimental Procedures

Partial transient liquid phase diffusion brazing of a copper-beryllium alloy (C17200) was performed with three Ag-based interlayers. The nominal composition of the base metal and interlayers are shown in Tables 1 and 2, respectively. The specimens were prepared using SiC paper down to 4000-grit finish then polished using diamond suspensions down to 1 µm.

After ultrasonic cleaning in acetone, the specimens to be joined and the Ag-based interlayers in the form of a 100-µm-thick foil were kept in ethanol to prevent surface oxidation effects. Before the brazing operation, a spreading test was accomplished to predict the wettability of the interlayers. In this test, the filler metal pellet of known volume was melted over the surface of the specimen for a specific time at 780°C under a fully controlled condition. The spreading factor (SF) was determined from the following equation (Ref. 12).

$$SF = \frac{\text{Total plan area wetted by the molten filler metal}}{\text{Original plan area of the metal pellet}} = \frac{\left(6V/\pi\right)^{1/3} - h}{\left(6V/\pi\right)^{1/3}} = \frac{D-h}{h} \qquad (1)$$

where V is volume of the interlayer, h is maximum height of the solidified filler metal pool, and D the diameter of sphere corresponded to volume of the metal pellet before spreading test. Because the geometry of the solidified interlayers was seldom perfectly circular, image analysis was used to provide an accurate measure of the wetting area. The method for measuring the height (h) was to determine the peak height from metallographic sections of profilometer traces and use a micrometer. With this technique, the melting and spreading processes can be separated so that fully isothermal experiments can be performed. The initial average roughness R_a of these substrates was 78±45 nm. The substrates used for wetting experiments were slightly polished with 3 µm diamond paste prior to the experiment. This polishing did not modify the initial roughness, but by removing mature passive films, it ensured a reproducible initial surface state. In the present investigation, along with the "spreading factor," a measurement sessile drop test was studied by the classical sessile drop technique. In the sessile drop experiment, interlayer droplets of 30 to 100 mg were prepared prior to the wetting experiment by vacuum arc remelting with the operation voltage of 60 V and 140–150 A. The wetting experiment was started with heating the droplets from room temperature to the selected brazing temperatures. The heating rate of the furnace was kept at 20°C/min. The changes in drop base radius R, height and contact angle θ of the drops was monitored during the test. After spreading and sessile drop tests, the joining operation and heat treating of the specimens were carried out in argon and vacuum atmospheres according to Fig. 1. A range of optimum temperatures, 720° and 780°C, was set as diffusion temperatures for different holding times. The heating and cooling rates were 20°C/min and 30°C/min, respectively. The uniaxial compression load of 0.5 MPa was applied along the longitudinal direction of the specimens. The microstructure of the reaction layer was examined using the optical and scanning electron microscope (Cam Scan 2300MV). The composition of the reaction layer was determined through an energy dispersive spectroscopic method. The operating voltage and stabilized beam current were maintained at 20 kV and 20 mA, respectively. The specimens were loaded in the microprobe such that the diffusion interface was perpendicular to the X-axis of the specimen stage and hence parallel to the electron beam. Specimens of the joint cross section were prepared by a common metallographic procedure using a Buehler Phoenix Beta grinder–polisher. To clarify further the phase composition near the interface of the interlayers and substrate, some specimens were cut from the transition region at the faying surface of the joints. The XRD analysis was carried out using the Cu Kα target at a working voltage 40 kV and current 150 mA.

Microhardness measurements at the interface of the base metal and filler met-

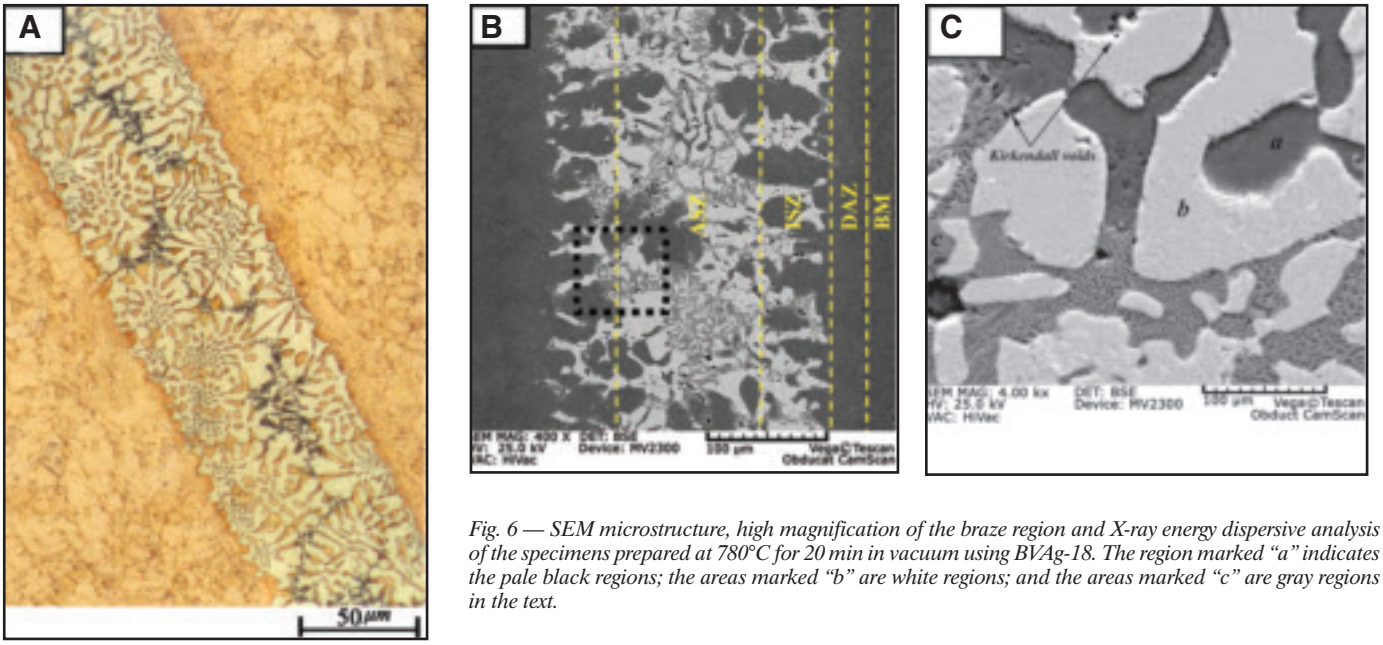

Fig. 6 — SEM microstructure, high magnification of the braze region and X-ray energy dispersive analysis of the specimens prepared at 780°C for 20 min in vacuum using BVAg-18. The region marked "a" indicates the pale black regions; the areas marked "b" are white regions; and the areas marked "c" are gray regions in the text.

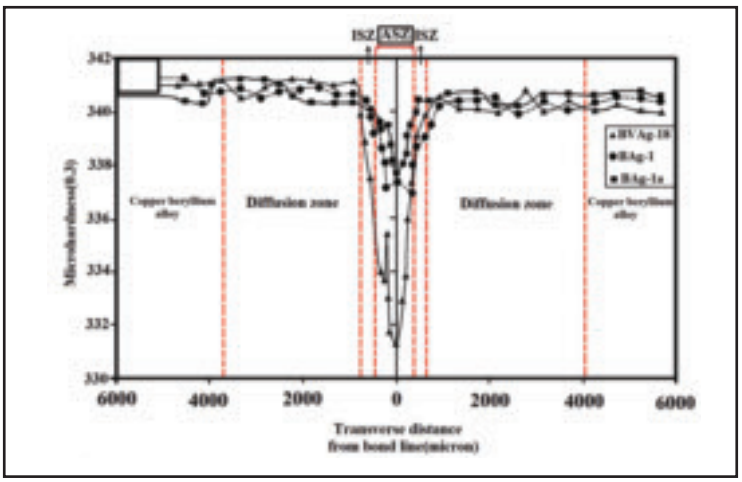

Fig. 7 — Microhardness profiles as a function of distance from the centerline for joints prepared at 780°C in a vacuum.

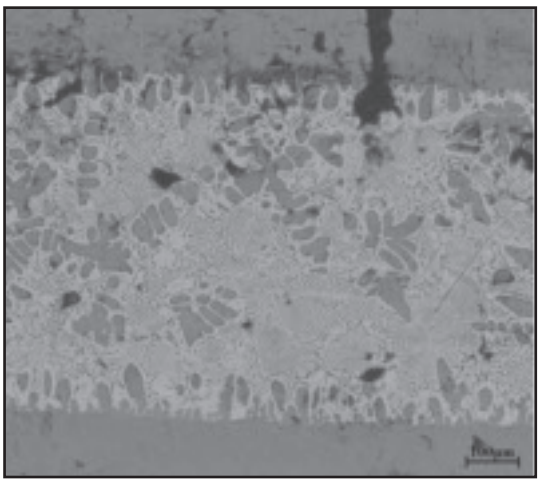

Fig. 8 — Presence of voids at the interface of joints fabricated in argon atmosphere.

Table 3 — Spreading Test Results

Pattern	Temperature (°C)	Volume	Filler metal height after wetting (mm)	Spherical diameter (mm)	Surface wetting factor
BAg-1	780	0.4537	2.3	8.1	0.71605
	720	0.3762	2.4	8.1	0.6913
BAg-18	780	0.3681	2.8	8.0	0.6500
	720	0.2432	2.6	7.2	0.6388
BAg-1a	780	0.4052	2.1	8.0	0.7375
	720	0.3853	1.9	7.1	0.7329

als were carried out with Vickers hardness scale. Tensile and fatigue tests were accomplished according to ASTM D1002-72 and ASTM D1002-64 at a strain rate of $3.28 \times 10^{-4}\ s^{-1}$, respectively (Refs. 13–15). Three specimens were tested for each joining condition and their averages were taken — Fig. 2. The fatigue test was performed with a lap scheme and for each point six specimens were examined. There was no machining or surface conditioning after the joining operation. This facilitated the testing of the joints without modifications to improve the joint quality by removing any discontinuity and overflowed material at the joint. Hence, the tested specimens were accurately the same as the actual joint, which was not altered after the joining operation. All tests were completed at room temperature in a servo hydraulic testing machine. The test bars were cut to 25.54 cm in lengths and held in hy-

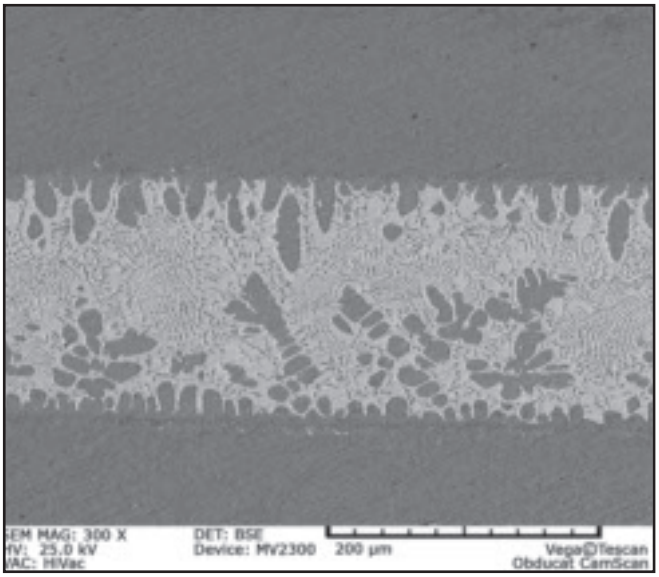

Fig. 9 — Microstructure of joints prepared at 780°C for 20 min in vacuum, showing a suitable joint without any voids and porosity at the faying surface of the substrate and interlayer.

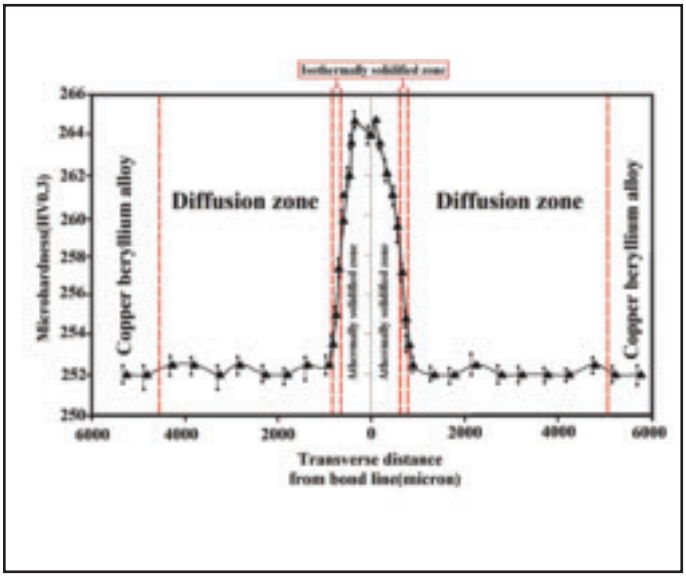

Fig. 10 — Microhardness of bonds fabricated at 780°C for 20 min without age hardening.

draulic grips. A simple load-controlled, ramp load/unload cycle was used with 18-Hz cycling frequency. All of the tests were performed with fully reversed cycling with zero mean stress or R= –1, where R is minimum load/max load. For fully reversed cycling R = –1 because the minimum load is equal to minus the maximum load. Before the fatigue test, all the specimens were subjected to an ultrasonic cleaning. The service stress was assumed to be ±12 MPa. However, the actual stresses being applied were involving a range of stresses and mean stresses. A succession of fatigue tests was run at different stress amplitudes, with numerous specimens being run at two of these amplitudes. The data of the S-N figure wereobtained with specimens that were believed to have the highest quality. The curve fit was drawn from the data points obtained at 0.09 GPa to 0.36 GPa, and the averages of numerous tests run at the lower and higher stress amplitudes.

Experimental Results and Discussion

Spreading Test Results

As a capillary joining process, partial transient liquid phase diffusion brazing is crucially dependent upon the ability of the liquid interlayer to spread in a stable fashion over the substrate surface. The liquid spreading temperature is also an important technical parameter since an excessively high joining temperature can affect the microstructure and properties of the copper-beryllium alloy. A spreading test showed that the filler metals have the ability to wet the base metal at some certain joining temperatures (Table 3). Spread area of BVAg-18 filler metal was inferior to that of BAg-1 and BAg-1a filler metals. However, the spread area of BVAg-1a with quaternary system was larger than BAg-1 at the same test temperature. It is believed that at the beginning of the process, when the new surface is formed, the concentration of the phases is uniform, with a discontinuity at the interface. The new surface is a sink for the surface-active molecules and then, an adsorption process starts, inducing a diffusion profile and allowing the system to reach its invariable condition (equilibrium or steady state) by

Table 4 — EDS Composition Taken across Joints Prepared at 780°C for 20 Min with BAg1a, BAg-1 and BV Ag-18

		Average Chemical Analyses (wt-%)								
Interlayer	Symbol	Sn	Cu	Be	Cd	Zn	Ni	Co	Pb	Ag
BAg-1a	a	—	78.51	—	1.56	1.00	0.02	0.01	0.01	18.10
	b	—	11.02	—	8.20	2.04	—	—	—	78.74
	c	—	72.46	—	26.32	—	—	—	—	1.22
	d	—	53.44	—	0.87	39.96	—	—	0.06	5.67
	e	—	1.24	—	0.53	64.19	—	—	—	34.04
	f	—	1.85	—	62.46	—	—	—	0.07	35.62
BAg-1	g	—	65.79	—	3.34	1.00	0.03	0.01	0.01	29.82
	h	—	14.02	—	8.47	3.16	—	—	—	74.53
	i	—	81.63	—	16.24	—	—	—	—	3.13
	j	—	51.89	—	0.18	34.17	—	—	0.02	13.24
BVAg-18	k	0.96	92.14	—	—	—	0.11	0.09	0.06	6.64
	l	1.47	56.75	—	—	—	0.02	0.01	0.01	41.74
	m	72.06	1.01	—	—	—	—	—	—	26.93
	n	1.21	70.69	—	—	—	—	—	—	28.1

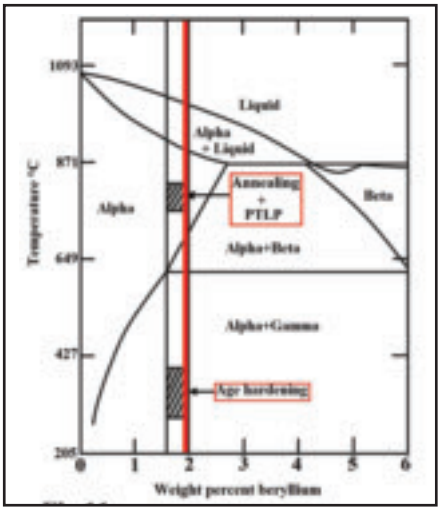

Fig. 11 — Cu-Be equilibrium phase diagram and steps of the brazing process.

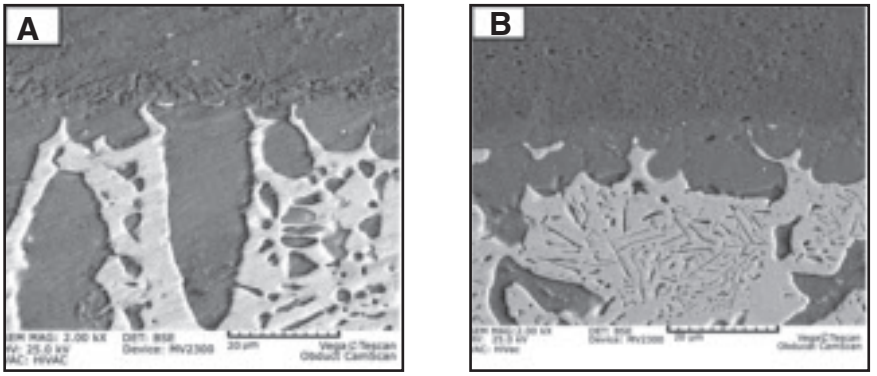

Fig. 12 — Details of the faying surface of specimens fabricated at 780°C using BVAg-18. A — 2 min; B — 20 min. See the growth of intermetallic layer and particles at the surface of the copper-beryllium alloy.

Table 5 — Thickness of the Interlayers for Specimens Fabricated at 780°C in Different Times

Brazing Time (min)	Interlayer Thickness (μm)		
	BAg-1a	BAg-1	BVAg-18
2	85±0.1	81±0.2	78±0.1
10	80±0.4	73±0.35	73±0.3
15	68±0.25	59±0.1	54±0.15
20	57±0.25	52±0.15	41±0.35

modifying the surface composition. The surface concentration varies until it reaches the equilibrium value corresponding to the disappearance of the diffusion profile or a stationary state.

Figures 3 and 4 present the results of the sessile drop test of the interlayers on the copper-beryllium alloy. The sessile drop tests demonstrated that the molten interlayers can effectively wet the base metal at 720° and 780°C. Figure 3 shows that the decrease of the wetting angle is less effective as the temperature is decreased from 780° to 720°C. However, excellent wetting of the substrate was achieved at 780°C in 15 min — Fig. 4. In view of the high number of constituents in the Ag-based interlayer systems, a 37–89 deg decrease in contact angle was observed. The sessile drop results indicated that the addition of Sn into the Ag-based interlayer significantly improved its wettability on the substrate. On the contrary, the increase of Cd additions into the Ag-based interlayer from 17.438 to 24.5 wt-% demonstrated no significant improvements upon the wettability of the molten interlayer on the substrate.

The present sessile drop test results support a body of phenomenological evidence that suggests alloying between the liquid phase and the solid phase is an important contributor to stable wetting. For example, Bailey and Watkins (Ref. 16) studied the spreading characteristics of a large number of combinations of liquid and solid metals and observed that stable wetting was produced when there was a degree of mutual solubility between the liquid and solid metals. In comparison, wetting was not produced when there was no significant mutual solubility. These findings were confirmed by Klein Wassink (Ref. 17) in which the addition of Pd to Ag spreading on iron resulted in enhanced spreading. It was proposed that the beneficial effect on wettability, of solubility between the interlayer and the substrate, is attributable to a reduction in the solid/liquid interfacial energy as a result of an increase in homogeneity across the interface. Thus, wetting can be improved by adding a relatively small amount of a suitable element like Sn and Cd to the interlayer. As a result, the spreading stage during which the wetting angle rapidly decreases is controlled by dissolution reactions at the liquid alloy/substrate interface.

Microstructures of the Joint Region

The effect of the interlayer composition on the rate of isothermal solidification was studied by SEM micrographs shown in Fig. 5. There are many reaction phases observed at the interfaces between the interlayers and substrate. Table 4 demonstrates that the alloying elements were dissolved into the molten interlayers at brazing temperature of 780°C. It was interesting that the consumption of Cu from the molten interlayers results in forming a Ag-rich matrix in the brazement. However, the formation of different intermetallic compounds during the brazing operation is significantly increased when the number of constituents in the Ag-based interlayer increased. From this result, it is inferred that the decrease of Cu from the Ag-Cu eutectic liquid results in isothermal solidification of the braze. It is evidenced by the formation of irregular intermetallic compounds due to solidification of the molten interlayers as illustrated in Fig. 5. An incomplete isothermal solidification of the liquid interlayer occurred in the specimen joined for the lower temperature. This resulted in the formation of continuously distributed eutectic constituents of Ag-rich and Cu-rich phases in the joint's centerline. Silver diffused from the interlayer, through the ternary solid solution, dissolving copper and forming silver-copper liquid along copper alloy grain boundaries.

In contrast to the situation at 780°C, using a Ag-based interlayer with a higher amount of Ag resulted in a semicomplete isothermal solidification. However, an increase in the brazing temperature resulted in formation of bigger eutectic constituents and solid solution in the joints. Diffusion products detached and flowed into the Ag-Cu liquid, and Ag dissolved along grain boundaries of the Cu substrate, forming Ag-Cu liquid. In the brazing-affected zone, secondary-phase precipitates were observed. The matrix present at the interfaces of the bonds is mostly Cu-rich solid solution containing Ag, Cd, Zn, and Sn resulting from the dissolution of the base metal and the interdiffusion of the alloying elements during the brazing operation. The analyses, however, suggest that Cu_3Sn and Ag_3Sn particles in BVAg-18 filler metal were precipitated in this zone — Fig. 6A. It is believed that the formation of the Sn-rich particles is directly associated with Sn diffusion out of the liquid into the base

metal. Figure 6B shows three distinct microstructural zones in the specimen brazed with BVAg-18 at 780°C. In the middle of the joint, athermally solidified zone (ASZ) is formed due to insufficient time for isothermal solidification completion. This zone can be explained by considering solidification sequence of remained liquid during cooling. In this area two of the main intermetallic compounds (Cu_3Sn and Ag_3Sn) were formed. Very close to ASZ, isothermally solidified zone (ISZ) was formed by interdiffusion between the substrate and interlayer during holding at the brazing temperature. The third zone is a diffusion-affected zone (DAZ), which consists of Sn precipitates due to diffusion into the base metal (BM) during the brazing operation. Dark microvoids were also observed within the bond region, with a dimension of 0.8–1.5 μm. It is believed that Sn is a faster diffusing species with respect to Ag (Ref. 18). Hence, the shift in braze interface results in the formation of Kirkendall voids. Furthermore, interdiffusion between the Cu substrate and the Ag-based interlayer caused protrusions at the interface. Enhanced diffusivity at the Cu grain boundaries accelerated the consumption of Ag with subsequent interaction layer breakdown. The melt is

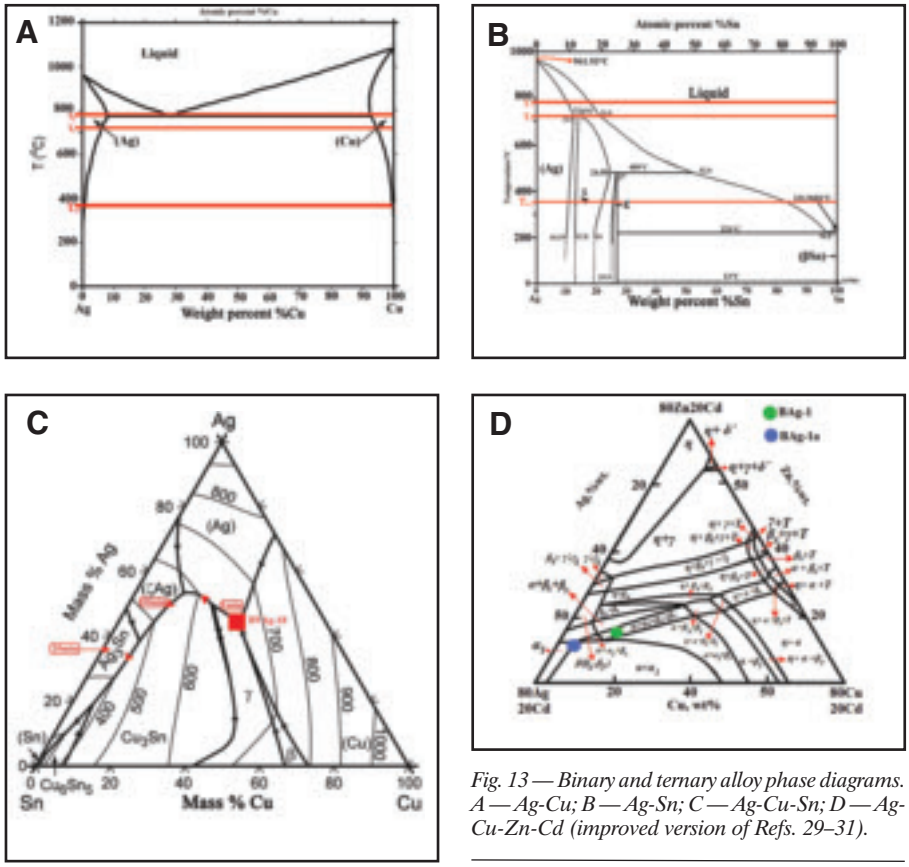

Fig. 13 — Binary and ternary alloy phase diagrams. A — Ag-Cu; B — Ag-Sn; C — Ag-Cu-Sn; D — Ag-Cu-Zn-Cd (improved version of Refs. 29–31).

Table 6 — Results from Tensile Tests on the Joints at Various Conditions

Interlayer Type	Brazing Temperature (°C)	Brazing Time (min)	Tensile Strength (MPa)		Ultimate Tensile Strength (MPa)	
			Argon	Vacuum	Argon	Vacuum
BAg-1	720	2	75.983	98.730	128.701	139.654
		10	76.163	99.052	131.672	143.007
		15	77.152	102.763	132.761	147.453
		20	77.786	105.896	138.856	148.453
	780	2	71.321	107.542	139.278	135.234
		10	71.872	110.432	142.563	137.820
		15	72.169	114.672	145.054	141.816
		20	79.067	118.520	149.563	154.675
BAg-1a	720	2	69.982	97.504	128.510	135.987
		10	70.342	98.692	131.342	137.562
		15	72.630	103.673	132.543	138.093
		20	77.652	104.872	133.780	138.982
	780	2	76.238	108.543	139.718	142.019
		10	77.753	112.218	142.763	149.630
		15	78.062	114.983	143.092	152.563
		20	78.521	118.456	147.786	153.870
BVAg-18	720	2	70.872	102.453	131.345	128.012
		10	71.872	102.732	132.764	137.118
		15	72.043	105.763	135.453	138.675
		20	74.984	111.234	140.065	149.832
	780	2	85.542	117.010	121.653	123.567
		10	86.098	119.097	137.789	140.654
		15	88.012	122.783	142.873	144.986
		20	88.205	123.077	151.333	156.450

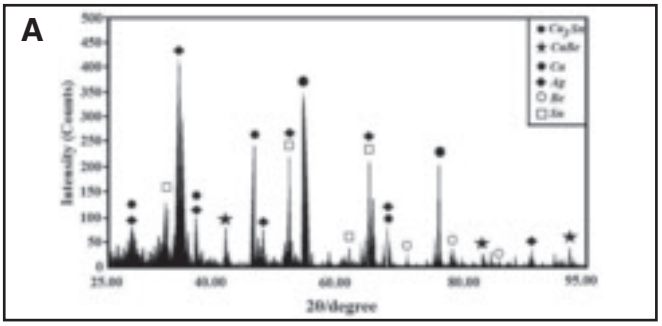

Fig. 14 — X-ray diffraction patterns near the interface of BVAg-18 interlayer/copper-beryllium alloy brazed at 780°C. A — 2 min; B — 20 min.

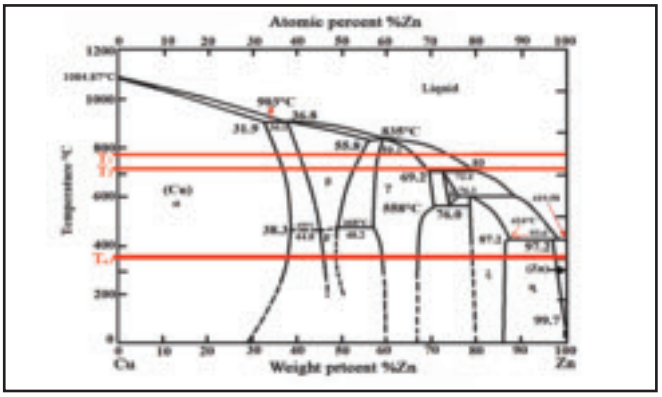

Fig. 15 — Binary alloy phase diagram of Cu-Zn.

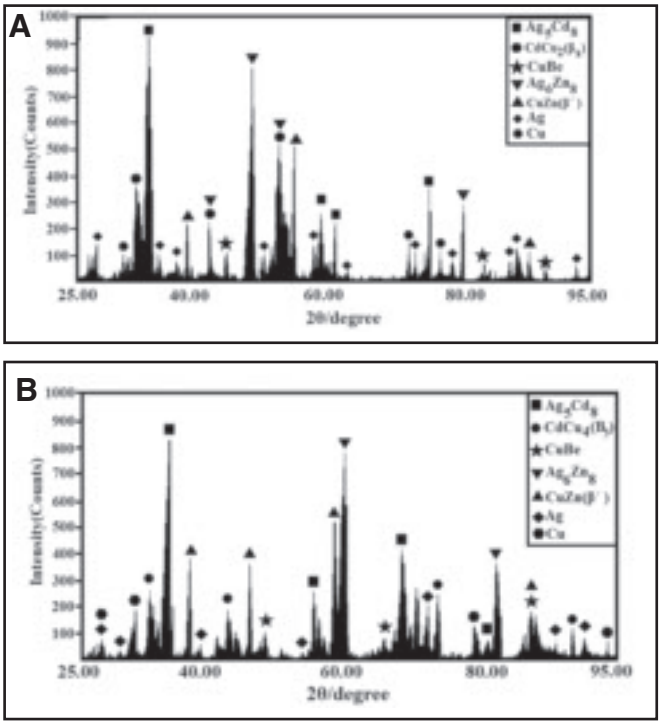

Fig. 16 — XRD spectra of specimens brazed at 780°C. A — BAg-1; B — BAg-1a.

enriched with Ag during the growth of the ternary solid solutions. The breakdown of the interaction layer causes dissolution of the Cu substrate. Thus, the Ag-Cu liquid regains Cu and its composition moves back toward the eutectic composition. Further dissolution also leads to a melt saturated with Cu. EDS analysis of the specimens from different regions in Fig. 6C showed that the pale black region consisted of 75% Cu, 19% Sn, and 6% Ag, while the white region included 74% Ag, 23% Sn, and 3% Cu. The third gray region is also evidence of a eutectic containing 52% Cu, 39% Ag, and 9% Sn. The combination of the phases is close to Cu_3Sn, Ag_3Sn, and Cu-Ag eutectic phases in the centerline, respectively.

Effect of Brazing Parameters

The optimum hardness was achieved for the specimens brazed at 780°C in a vacuum of 15.001×10^{-2} torr — Fig. 7. Lower hardness of the specimen brazed with BVAg-18 at the centerline nearby the isothermal solidification zone might be attributed to the absence of intermetallics and the presence of Ag-rich solid solution resulting from the dissolution and interdiffusion. The highest microhardness at the bond region is related to the specimens brazed with BAg-1a. This fact is attributed to a large amount of the intermetallics in comparison with those brazed with BVAg-18. Furthermore, lowest and highest microhardness were 331 and 341 HV, respectively. It is important to note that voids and porosity were observed in the joints fabricated in argon atmosphere — Fig. 8. These voids were formed because of oxidation of the base metal and interlayer with argon impurities during the brazing process. The same results obtained in another research (Ref. 19) showed that the presence of surface-oxide at the moving solid-liquid interface prevents the complete metallic contact at the braze surface. This has been verified by joining of the copper-beryllium alloy under vacuum atmosphere — Fig. 9. The optimum condition exhibits a good bond along the joint's interface, and it was free from discontinuities and microcracks. It is noticeable that the Kirkendall voids appeared as soon as the intermetallics expanded. The Kirkendall void formation would be facilitated by applying argon atmosphere and entrapping impurities at the faying surface of the braze. However, the growth rate constants for the formation of the intermetallics are related to integrated interdiffusion coefficients and activation energies for the formation of the intermetallic compounds in various brazing atmospheres.

The base metal hardened by heating the supersaturated solution to 316°–350°C and holding for 2–3.5 h to precipitate the γ phase. Adding Co in the base alloy promoted a fine grain size by limiting grain growth during solution annealing, and made precipitation hardening less sensitive to time. For a given brazing time, the hardness increases with increasing the distance from the joint centerline. The higher hardness of the joints in the diffusion-affected zone can be attributed to the higher diffusion of the alloying elements, e.g., Ag and Sn. Figure 10 shows the microhardness of the bonds without age hardening. As it is seen, the age hardening had a significant effect on the hardness of

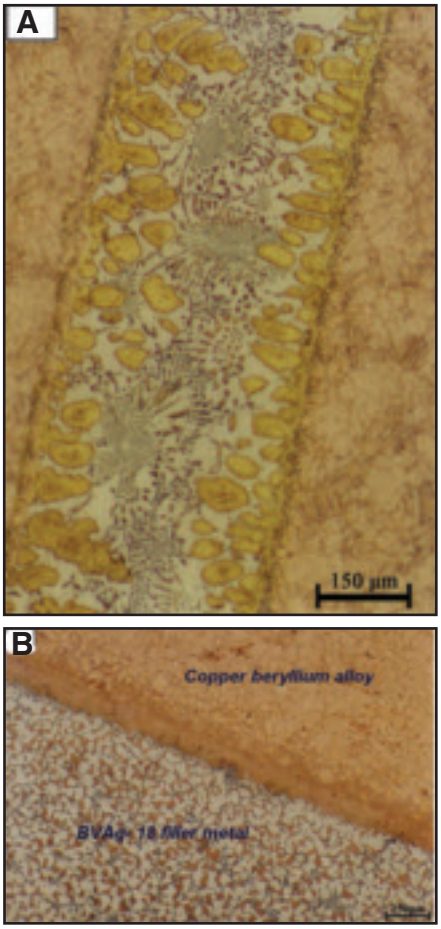

Fig. 17 — Microstructure of specimens prepared at 780°C for 20 min. A — Brazements prepared with BAg-1a; B — brazements prepared with BVAg-18. See diffusion paths in the copper-beryllium grain boundaries and eutectic pockets at the mating surface of the substrate and interlayer.

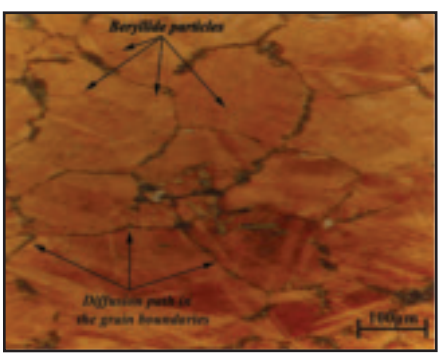

Fig. 18 — Diffusion of the brazing products and melting point depressant into the grain boundaries.

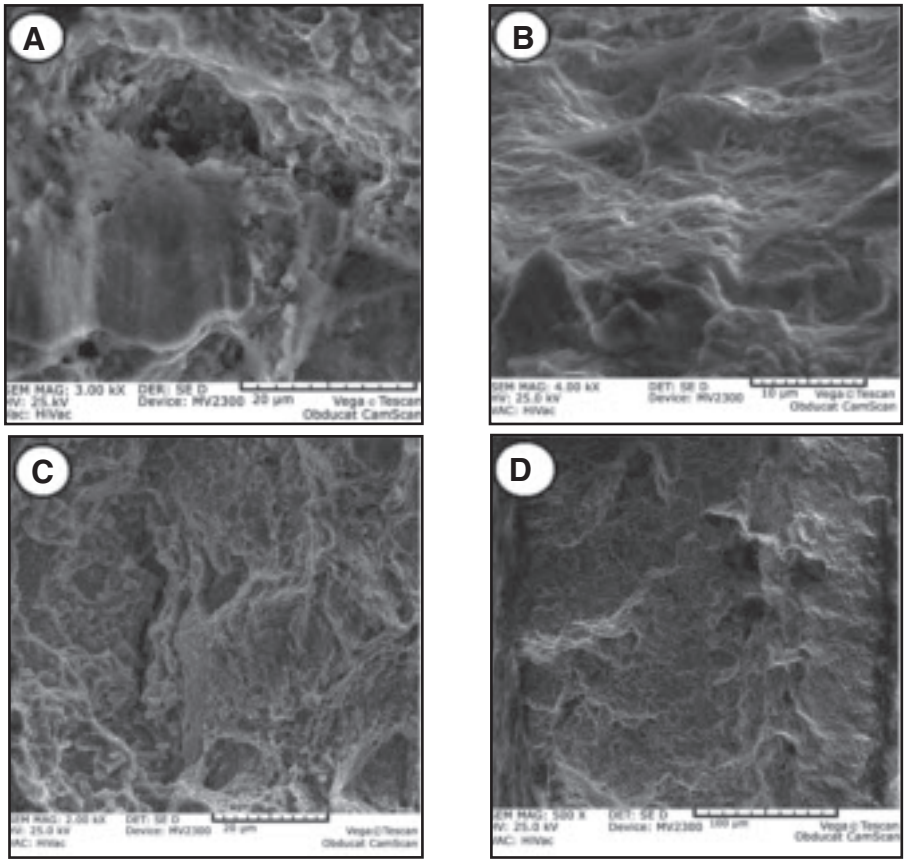

Fig. 19 — Fractography of the bonds after the fatigue test, prepared by BVAg-18 at 780° C. A — 20 min, high stress; B — 10 min, high stress; D — 10 min, low stress.

the brazements, especially on the base metal. The precipitation hardening stages of the copper-beryllium alloy can be written as follows:

Supersaturated solid solution (α)→
GP Zone → γ'' → γ' → γ

where α is solid solution and γ is a brittle phase with combined formula CuBe. In the base alloy, beryllium was dissolved in α phase, and then trapped in the solid solution networks. This was another reason that the hardness of the joints after brazing increased by forming new brittle phases — Fig. 11. It should be pointed out that aging treatment after the brazing operation had a considerable effect in the homogenization of the alloying elements.

The average composition of the solute was increased as a function of time during the precipitation hardening operation. It is believed that as the aging time increases, the length and width of the Cu-Be precipitates increases significantly. Therefore, it is expected with increasing the holding time in the aging treatment, the alloy exhibits higher hardness. However, the EDS analysis could not analyze the Be content in the braze line or base metal. It is clear that the Be, as well as other elements in the substrate, was dissolved by the molten interlayer during the brazing operation. This analysis cannot be determined unless a high-resolution transmission electron microscopy is used to reveal metastable γ' phase and its matrix orientation in the specimens. This objective will be addressed in the next investigation of the brazed specimens. P. G. Shewmon (Ref. 20) derived the following equation to describe the effect of precipitation time on the average composition of the solute.

$$\bar{C} = C_0 \exp\left[-\left(\frac{2Dt_{aging}}{r_e^2\left(\frac{C_p}{C_0}\right)^{1/3}}\right)^{3/2}\right] \quad (2)$$

where C_0 is the initial concentration of the solute in the matrix, r_e the radius of equivalent sphere volume of a precipitate, D the diffusion coefficient of the solute, and C_p the concentration per unit volume of the solute in the precipitate. In this regard, assuming that coarsening of the CuBe was controlled by the bulk diffusion and the overall diffusivity depends on the diffusion of Be, the calculated r_e value for CuBe is 118 nm. It is conceivable that if r_e increases, the rate of participation increases. Consequently, the growth of randomly distributed precipitate particles yields an increase in hardness. The solid solution decomposition proceeds through the diffusion process characterized by high diffusion coefficients in higher aging time, and the precipitates grow further by absorbing the solute atoms nearby, leading to the higher hardness.

The result of this study is in agreement with recent experimental achievement in

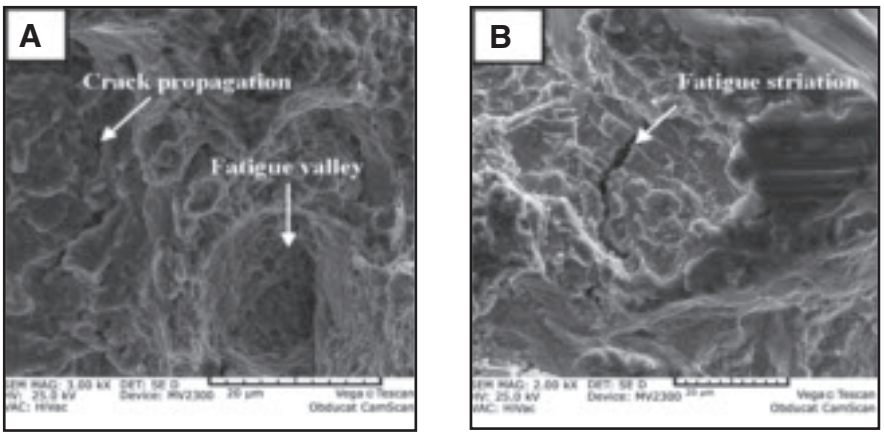

Fig. 20 — Micrograph of fracture surface for joints fabricated at 780°C for 20 min. A — ductile fracture; B — brittle fracture.

analyzing the aged alloy by high-resolution transmission electron microscopy. In this view, Yagmura et al. (Ref. 21) found that the length and width of plate-like precipitates in the Cu-1.9Be alloy increased from 10–20 to 50–100 nm and 2–5 to 10 nm, respectively, along the trace of the habit planes. In this case, however, the supersaturated solid solution decomposes in two different ways. Continuous precipitation occurs throughout the whole matrix due to local compositional fluctuations leading to the nucleation of the second phase or to spinodal decomposition. This system shows preferential nucleation of the second phase at particular locations like grain boundaries or triple junctions. The heterogeneous precipitation leads to formation of a two-phase colony that grows behind a migrating boundary such that the composition and orientation of the matrix phases across the reaction front changes discontinuously (Ref. 22). The discontinuous precipitates are usually formed behind a moving grain boundary, which advances into the supersaturated matrix. Then, the supersaturated matrix decomposes into a two-phase lamellar structure comprising a solute-depleted matrix and discontinuous precipitates (Ref. 23). In the brazing system, Ag was regarded as a ternary element to enhance the mobility of the reaction front and simultaneously the growth rate of the discontinuous precipitates at the diffusion-affected zone. It can be said that there is a large driving force to move the boundary for preeminent position and thus, minimum interfacial energy of the precipitate facet. The coherency strain energy provides this driving force and controls discontinuous precipitation. Surface morphology is another driving force for the initiation. Therefore, when the coherency strain energy decreases, other energy contributions like the interfacial energy become increasingly important and possibly dominate the discontinuous precipitation reaction in the alloy and brazing zone.

In perspective of the brazing, it can be inferred that diffusion of Ag and Sn with high diffusivity from the BVAg-18 interlayer into the substrate is an isothermal solidification rate controlling factor. Thus, an increase in the diffusivity of the elements with an increase in the brazing temperature causes a swift plunge in the isothermal solidification time. Alternatively, continual interdiffusion of the elements between the liquid interlayers (BAg-1a and BAg-1) and the base metal continually modified the composition of the liquid as solidification progressed. At any given instant, the concentration gradient of the diffusing solute in the base metal is influenced by the solute solubility limit, and thus, the change in concentration gradient with distance is dependent on the maximum solute solubility (Ref. 24). Therefore, the diffusion-controlled isothermal solidification rate is not only dependent on the diffusion coefficient, but also on the solubility, both of which can be influenced differently by the brazing temperature. An increase in the temperature will cause an exponential increase in the solute diffusivity according to the Arrhenius equation. Elemental diffusion of the base alloy can be improved by increasing the holding time. To prove the effect of time on the quantity of dissolved solid metal, Lashko et al. (Ref. 25) proposed that increasing holding time exponentially affects the quantity of the dissolved metal. In contrast, it is believed that the mobility of Cu in the Sn-containing phases is extremely rapid and anisotropic due to its fast diffusion by an interstitial mechanism, indicating the possibility of diffusion of the copper atoms from the base metal into the interlayers and at the meantime a decrease in the amount of liquid maintained at the brazing temperature due to the loss of the melting point depressant solute causes isothermal solidification to occur by migration of the liquid-solid interface (Refs. 26, 27).

On the other hand, an interfacial chemical reaction can effectively be regarded as mass transfer or absorption of one phase by another across the interfacial region. Mass transfer across the interface resulted in a net decrease in the free energy of the system in order for the reaction to proceed. In the first moments of the formation of the interface, just the interfacial region was involved in any chemical reaction, and the decrease in the free energy of Cu-based alloy/Ag-based interlayer can be largely attributed to the decrease in the specific interfacial free energy (Refs. 28, 29). The variation of interfacial free energy with time during chemical reaction between two phases causes chemical composition gradient in front of the interlayer interface. Additionally, the interfacial energy becomes positive as the chemical reaction between the alloying elements in the interlayers and base metal approaches chemical equilibrium. This occurs because phases, which must come to equilibrium, are more stable than the interfaces.

Lowell and Chalmers (Ref. 30), though, theoretically examined the dissolution of solid in liquid and indicated that in an unstirred liquid system, movement of the solid-liquid interface was dependent on the square root of the holding time and that the boundary layer thickness also increased in a similar manner. The results of this study were in agreement with the results of the mentioned research. It means that at the higher temperature as the brazing time increased, the interlayer thickness significantly decreased (Table 5). As it is seen from Table 5, increasing the brazing time from 2 to 20 min has a considerable effect on the interlayer thickness. This can be attributed to distribution of Ag, Cd, Zn, and Sn in the mating surface and diffusion zone. However, subsequent heat treatment caused a redistribution of these elements, resulting in compositional homogeneity across the joint region. For example, details of the faying surface of the specimens made by BVAg-18 at 780°C for 2 and 20 min are shown in Fig. 12. It is important to note that selecting the appropriate brazing temperature to achieve a specified maximum concentration of the interlayer at the joint is dependent on the isothermal solidification. Since the brazing temperature is dependent on the amount of melting point depressants that are to be diffused away into the substrate, the brazing temperature is dependent on this equilibrium width.

In two of the filler metal systems, partial transient liquid phase diffusion brazing involves more than the dissolution of the base metal and its isothermal solidifi-

cation that accompanies diffusion of the solute. Since the interlayers with compositions of Ag54.56Cu15Zn16Cd17.438 and Ag44.5Cu15Zn16Cd24.5 were used, the solidification of the brazing layer of the specimens is proeutectic and eutectic types according to the phase diagrams of these alloys — Fig. 13A–D (Refs. 31–33). The concentration of Zn in the vicinity of the copper-beryllium alloy becomes very low compared to that of Cd. These conditions are conductive to the formation of regions containing some Zn-eutectic phases at room temperature depending on local concentration of Ag and Cd, in these regions. Zn and Ag form eutectics with Cu at the brazing temperatures. The formation of these eutectic phases is expected based on the phase diagrams shown in Fig. 13A and B. Figure 13C shows the liquidus projection of Ag-Cu-Sn ternary alloy phase diagram and the important reaction scheme is also included. According to Fig. 13C, there is a huge miscibility gap among the liquids. The molten interlayer tends to separate into two liquids. One is rich in Ag, and the other is rich in both Cu and Sn. It is expected that the formation of interfacial AgCu, Cu_3Sn, and Ag_3Sn results in isolation of the molten interlayer (BVAg-18) and substrate. As evident from the Cu-Sn binary alloy phase diagram (Fig. 13B), the solid solubility of Cu in Sn is negligibly small, while in the liquid state it is significant. Hence, the Cu partially dissolved in the molten interlayer, particularly in the solute boundary layer, must precipitate during cooling. This precipitation usually takes place on the existing grains in the intermetallic compound. The preferred precipitate is the ξ-phase in accordance with the equilibrium diagram. If the intermetallic itself is ξ, then it may not be easy to distinguish between the crystals that form during the isothermal reaction and those that precipitate on cooling. It is believed that Sn of the BVAg-18 interlayer reacts with Cu to form intermetallic compounds at the interface during the interlayer reflow process. Formation of the intermetallic compounds is imperative for good wetting and brazing, although there are many other reasons for a suitable wetting, including capillary flow, relative attraction of the atoms of the liquid to each other and to those of the solid, fluidity, viscosity, vapor pressure, the presence of oxide films, the extent to which alloying is affected by the thermodynamic properties of the brazing atmosphere and gravity. However, Sn diffused dramatically into the base metal and migrated to the grain boundaries. The solute distribution in the boundary layer, where the concentration of Cu is highest near the interlayer, would have favored nucleation on the intermetallic grains. It can be assumed that the interfacial reaction produced Ag_3Sn and Cu_3Sn intermetallics and stopped once the Sn remaining had been consumed completely (Ref. 34).

Observations of the present study showed that both the Ag_3Sn and Cu_3Sn are found at the interface between the BVAg-18 and substrate as demonstrated in Table 4 and Fig. 5C. In addition, the Ag-Cu eutectic dominates the joint. It should be noted that recognition of the intermetallics only by image contrast and EDS analysis was very hard as the size and shape of the compounds were very small and similar; therefore, XRD analyses were performed to recognize the intermetallic compounds in the bond area. XRD analyses revealed that the microstructure of the specimens brazed with BVAg-18 consists of Cu_3Sn and Ag_3Sn solid solutions, and the amount of the compounds increases with increasing brazing time from 2 to 20 min — Fig. 14. During the brazing operation, the isothermal solidification is mainly controlled by the diffusion of Ag and Sn in the solid base metal. With Ag the liquid layer continually diffused into the base metal, the liquid composition immediately adjacent to the base metals becomes Cu-impoverished and Ag-enriched results in an increase in the melting temperature and eventual isothermal solidification. In this stage, the joint was formed by isothermal solidification and solidification of liquid layer during cooling when isothermal solidification was not complete. The microstructure of isothermal solidification zones immediately adjacent to the base metal was mainly a Cu-solid solution, whereas the eutectic containing Ag solid solution and Ag-Cu eutectic phases solidified in the center of the joint during cooling.

It was also observed that the amount of Ag-Cu eutectic in the joint increases with increasing brazing time from 2 to 10 min (see the diffusion path in Fig. 13C). Increasing the brazing time increases the contact area and also enhances the diffusion of Ag and Sn into the base metal, which accelerates interlayer dissolution. When the brazing time was increased, isothermal solidification governed joint formation due to the change in the liquid phase composition and form intermetallic compounds. The diffusion of Ag and Sn into the solid results in a change in joint composition at the brazing temperature and this prompts isothermal solidification. Figure 14 shows that with increasing the brazing time, the intermetallic compounds start to form and during the isothermal solidification, Ag_3Sn and Cu_3Sn dominated the metallic bond line. At a brazing temperature of 780°C, a large amount of Ag and Zn were diffused from the interlayer to the Cu substrate when BAg-1a was used as an interlayer. However, the concentration of Ag in the vicinity of the copper-beryllium alloy becomes very low compared to that of Zn. Cu and Zn form eutectic and proeutectic with Ag at temperatures of 780° and 720°C, respectively, which are below the melting point of either the Cu substrate or the interlayers — Fig. 15.

On the other hand, in specimens brazed with BAg-1, the intermetallic compounds containing Ag, Cu, Cd, and Zn were formed in a compact layer near the base metal. Apparently these elements formed $CdCu_2$ (β_x), $CdCu_4$ (β_y), Ag_5Cd_8, Ag_5Zn_8, and CuZn (β'). At temperature of 780°C, the concentration of Ag was very high, compared with that of Zn in the substrate. As can be seen from Table 4, the Zn concentration altered dramatically in the area *e* as a result of forming an intermetallic. As indicated in Table 4, the phases formed in joints bonded with BAg-1a and BAg-1a are mostly Ag-Cd, Cu-Cd, and Ag-Zn-based compounds, which are stable not only at room temperature but also at 780°C. So it was expected that the formation of these phases was closely related with an isothermal solidification and a subsequent solid-state interdiffusion between the base metal and molten liquid during the isothermal holding at the brazing temperatures. However, for joints fabricated with BAg-1 and BAg-1a, the $Ag_3Cd_7Cu_4Zn_{16}$ (T) phase cannot be observed at room temperature because it was transformed to other phases during the cooling. This can be inferred by the equilibrium Ag-Cu binary and Ag-Cu-Zn ternary alloy phase diagrams — Fig. 13A and D.

XRD results as shown in Fig. 16 confirm the existence of the CuZn (β') in the faying surface of the joints fabricated with BAg-1 and BAg-1a at the higher brazing temperature. It can be inferred that since Cu is the dominant diffusion species and Zn is highly reactive, Cu reacts with Zn and leaves Cd behind. It can be seen from Fig. 5 that the microstructures obtained by BAg-1 and BAg-1a consist of many distinct phases mainly mottled-gray and dark zones. In the specimens brazed with BAg1a, one of the zones is Ag poor (dark zones). The average chemical composition of this region is 51.80% Cu, 30.17% Zn, and 18.03% Ag. It can be observed that the dark zone has less Ag, higher Cu, and equal Zn contents compared to the nominal composition of the interlayer. On the other hand, the Ag-rich matrix includes 59.38% Ag, 19.59% Cu, and 21.03% Zn. It is clear that Cu content is increased in the dark zone while the Ag content is increased in the matrix. As shown in Fig. 5A and B, if the Ag content of the interlayer is increased from 44.5 to 54.56, the dark zone becomes smaller. Cd content decreases the size of dark zone and makes it smaller. Cd additions to a Cu-Ag alloy (BAg-1) reduce still further the temperature for the onset of solidification.

In this case, it is clear that the matrix with 41.89% Ag, 23% Zn, and 21% Cd is

Ag rich. Nevertheless, the dark zone in the matrix consists of 18.21% Ag, 32.56% Zn, and 9.78% Cd, and they are Zn rich. It was also seen from Fig. 5A and B that Ag and Cd poor regions are uniformly distributed in the matrix. This observation supports the prediction made from X-ray diffraction analysis in Fig. 16. It should be noted that CuBe observed in the analysis is in the vicinity of the substrate, in the isothermally solidified zone (ISZ). It was diffused away from the base metal matrix and entered into the molten interlayer. On the contrary, at the center part of the interlayer, CuBe was not observed. Furthermore, presence of the second-phase particles within the base alloy at the joint-substrate interface slow down the solidification process resulting in increasing the time required to prevent the formation of eutectic-type microconstituents at the joint (Refs. 35, 36). Based on the Ag-Cu, Ag-Sn, and Cu-Sn diagrams (Fig. 13A, F), liquidus concentration reduces with increasing the brazing temperature, which implies that for the initial filler alloy composition close to the eutectic value, more base material required to melt back into the liquated filler in order to dilute the liquid to attain equilibrium composition. As it was observed, the eutectic was formed from residual liquated insert during cooling from the brazing temperature due to insufficient diffusion of the solute, Ag, away from the liquid to achieve complete isothermal solidification during the holding time. However, it is believed that during aging, some of the intermetallic particles grow as a function of the square root of time (Ref. 37).

Tuah-Poku et al. (Ref. 38) provided a model for estimating the time to complete isothermal solidification based on simplifying assumptions that each surface of the base metal is semi-infinite and is covered by a layer of solute or melting point depressant (in this case, Ag, Cd, Zn, and Sn) whose composition at the solidifying interface is maintained at the solubility limit of the solute in the base metal at the brazing temperature. It was deduced from the analytical and numerical models that an increase in the brazing temperature simultaneously reduces the solidus temperature (solid solubility), and, thus, will tend to increase the time required for complete isothermal solidification. This indicates that the brazing time may not continue to monolithically decrease with increase in the brazing temperature but instead will tend to increase as the temperature reaches and exceeds a critical value where the influence of reduced solubility prevail higher diffusivity. Enrichment of the liquated Ag-based interlayer with Zn and Cd, capable of depressing the melting temperature, may not only be responsible for the reduction in isothermal solidification rate during the brazing operation. Interplay between an increase in diffusivity and decrease in solubility of melting point depressants with increase in temperature could be another important factor contributing to the observed reduction in the isothermal solidification rate at the higher temperature was consequence of prevailing effect of lower solubility of Cd and Zn relatives to their higher diffusivity. Therefore, the decrease in Cd and Zn solubility with decreasing isothermal solidification time at the higher temperature is an important factor to optimize partial transient liquid phase diffusion brazing of the copper-beryllium alloy. In this case, however, dissolution stage occurred at the preliminary steps of the brazing because the solute concentrations at the interface vary with the brazing time and the brazing temperature. Nakao et al. (Ref. 39) examined isothermal dissolution during the brazing process based on the Nernst-Brunner (Refs. 40, 41) theory, and they found that intermetallic phases that might form between the composition of the low melting point constituent and the final primary metal solid solution can hinder the dissolution process.

As shown in the Ag-Cu phase diagram, the solubility of Cu in Ag decreases with increase in temperature above the eutectic temperature. A reduction in the solubility of Ag at the higher temperature could cause a decrease in the rate of change of concentration gradient in the base metal. This could, according to Fick's second law, reduce Ag diffusion and, as such, decrease the rate of isothermal solidification at the higher temperature. Based on the theory of Nernest-Brunner, the thickness of the liquid boundary film at the shared interface is of the order of $2\sqrt{D_L t}$. This can prove that more given time will increase the concentration of Zn and Sn in the diffusion zone, and it could finally cause undesired phases at the bond interface.

Sinclair et al. (Ref. 42) suggested that in most situations, in contrast to the binary case, the composition of the liquid is required to change continuously as isothermal solidification progress. Therefore, if the solubilities or diffusion coefficients of the two solute elements in the liquid interlayer are very different, the solidification stage will be divided into two parabolic regimes. The first regime would be dominated by the faster solute, and the second dominated by the slower diffusion solute in the liquid. In addition, it has been suggested (Ref. 43) incomplete isothermal solidification might be due to the presence of a second solute, which might be present as an impurity in the base metal or in the interlayer, or more importantly in the mating surface of both. An enrichment of the liquid interlayer at the brazing temperatures with the interlayer solute elements such as Cd, Zn, Ag, and Sn, and a continuous modification of the liquid interlayer composition were observed as the solidification progressed. It is implied that a process of partitioning of the interlayer solute elements enriching the residual liquid interlayer occurs simultaneously as the isothermal solidification progress.

Effect of Grain Boundaries

Since partial transient liquid phase diffusion brazing of the copper-beryllium alloy is a diffusion controlled process, any factor that affects diffusion will change the process kinetics during the brazing operation. The most important case after isothermal solidification stage is grain boundary diffusion. The diffusivity is much higher at the grain boundaries of the copper-beryllium alloy than in the matrix when the brazing temperature is in the range of 0.6 to 0.7 of the equilibrium melting temperature. The grain boundary provides the most prominent diffusivity paths for the base alloy during the brazing operation. It is observed that the elements of the interlayers and ending products of the brazing process were penetrated into the base metal through the grain boundaries as shown in Fig. 17. These variations of shape of interface between the base metal and the interlayers can be attributed to the capillary force at the grain boundary during liquid state diffusion process. It was observed that grain boundary diffusion is expected to be dominant at the brazing temperatures. Since Ag atoms have higher diffusion rate in the molten interlayer, they can diffuse out of the way and thus allow the Ag_3Sn to grow. This can cause the pinning of grain boundaries by the Ag_3Sn resulting in a brittle diffusion zone. The intermetallics were found to form an almost continuous network distributing at grain boundaries. Diffusion of the main elements causes a big division at the shared surface of the base metal and interlayers. Fig. 17A and B show the effect of BAg-1a and BVAg-18 on this dissection, respectively. However, since the concentration gradients in the solid and liquid phases are highest near the substrate/interlayer, it can be shown that the lattice diffusion length needs to be only a little larger than the spacing d between grain boundaries of the copper beryllium alloy:

$$X_l = 0.7679(Dt_b)^{0.43} \geq d \qquad (3)$$

Then, the diffusion borders around neighboring grain boundaries overlap and a diffusing atom may visit many grains and grain boundaries during partial transient liquid phase diffusion brazing. From the macroscopic perspective, the base alloy

latter represents a weighted average of the lattice diffusivity and grain boundary diffusivity (Ref. 44).

It was shown by Zhou et al. (Ref. 45) that the liquid phase in the bulk region far from the grain boundary is smaller when the influence of grain boundary energy and liquid/solid interfacial energy are taken into account. Thus, the isothermal solidification process in the bulk material is accelerated when the effects of the grain boundary energy and the liquid/solid interfacial energy are taken into account. MacDonald and Eagar (Ref. 46) observed isothermal solidification in the partial transient liquid phase brazing of very fine grained (20 μm) base metal substrates. It was found that grain boundary grooving evolves into spherical protrusions as the growth process favors the elimination of regions of high curvature next to grain boundary cusps. Moreover, the kinetics of isothermal solidification and grain boundary grooving were suggested to be on the same order of magnitude. In large-grained samples (250 μm), the tendency to form protrusions is less. Results show faster interface kinetics in fine-grained specimens when compared to coarse-grained specimens. Grain growth was also observed to occur in fine-grained specimens. In the present investigation, average grain size is not more than 20 μm and grain boundary grooving observed at the mating surface of the alloy. This shows that the copper-beryllium alloy is likely to absorb diffused elements by its grain boundary diffusion paths. In addition, the grain size was relatively fine due the dispersion of the beryllides. The beryllide particles can be seen roughly spherical and dark blue in the matrix — Fig. 18. The macrostructure in Fig. 18 indicates that a significant amount of Ag-rich liquid entered the grain boundaries when Sn was present. The liquid phase has a propensity to wet the grain boundary once it lowers the interfacial grain boundary energy (Ref. 47). This thermodynamic driving force would not favor liquid thickness beyond several micrometers (Ref. 48). However, the Ag-rich liquid always was present at the grain boundary junctions. The presence of Sn in the liquid phase could help insert atoms of liquid into the grain boundaries. It was showed that faster grain-boundary diffusivity could help dislocation climb down, which assisted the penetration propagation (Ref. 49). Furthermore, Sigle et al. (Ref. 50) indicated that the grain boundary is weakened after inserting three layers of atoms of liquid because of the weakened bonds among the atoms, which increased the tendency for grain-boundary sliding and the formation of liquid channel thereafter. The bonds between Sn-Sn were believed to be much weaker than the bonds between Cu-Cu, which is related to the significantly lower melting point of Sn. It then can be speculated that the presence of Sn in the grain boundaries would assist the gliding of a grain boundary and therefore the later formation of channel and broadening of a grain boundary. It means the stress-induced diffusion of the Sn atom in the grain boundaries and the weak bond strength could result in significant grain-boundary penetration (Ref. 51).

On the other hand, MacDonald and Eagar (Ref. 46) found that the isothermal solidification rate of a fine-grained specimen was twice that of a coarse-grained specimen. In this view, irrigation of the base metal by composition dependent diffusion enhancement was occurring along the grain boundaries as the base alloy accounted to be a fine-grain material. The rate of isothermal solidification was qualitatively shown to be higher in fine-grained samples vs. coarse-grained samples (Ref. 52). Saida et al. (Ref. 53) studied the influence of base metal grain size on isothermal solidification rates. K. Ikeuchi et. al (Ref. 54) also showed that the grain boundary energy and the liquid-solid interfacial energy produce a chemical potential along the liquid-solid interface. This gradient of the chemical potential causes differential flow along the liquid-solid interface and, consequently, gives rise to migration of the liquid-solid interface. This demonstration also proves that the velocity of the liquid-solid migration increases for the interlayer with higher amount of Ag and Sn. It is also inferred that increasing the diffusion coefficient in the liquid phase accelerated the dissolution process. In this case, two factors are able to enhance the faceting of the solid/liquid interface: adsorption of certain types of intermetallics and brazing temperature (Refs. 55, 56). However, some of the intermetallics dissolved in the solid strongly promote the faceting of solid surface in vacuum and of grain boundaries. The brazing temperature decreases the mobility of the facets, slow down the equilibration rate of the grain boundary with the intermetallics contained in the liquid and enhances the faceting of the shared surface of solid and liquid. All these trends promote a rapid penetration of the liquid along grain boundaries.

Tensile and Fatigue Analyses

Tensile test results showed that weakest tensile strength of the joints occurred for the specimens prepared in argon atmosphere. For this case, voids within the bond region were responsible in weakening of the joint area. Table 6 shows the relationship between tensile strength of the joints and diffusion brazing atmosphere. Note that brazing at 780°C for 20 min under argon atmosphere, followed by aging at 350°C for 3 h resulted in a significant drop in tensile strength to 151.3 MPa. This suggests that the brazing atmosphere can lead to a decrease in strength of the base metal. It is obvious that the joint strengths for the optimum condition are quite different at the brazing temperatures, ranging from 128.012 to 156.45 MPa. Owing to the fact that the compositions at the interface are within the respective solubility limits, the increase in the strength of the specimen is due to the solid solution strengthening at the interfaces. It is also observed that the deformation during partial transient liquid phase diffusion brazing increased from 1.87 to 11.08% with an increase in temperature from 720° to 780°C. In all optimum specimens, joined with BVAg-18, failure was observed outside the joint interface close to the diffusion zone indicating that the diffusion-affected zone was the weakest within the joint. The plot about the strength also shows that strength of the specimens strongly depended on the brazing temperature.

In the copper-beryllium alloy, however, a critical brazing temperature was expected due to interplay between increase in diffusivity of the interlayer elements and increase in maximum widening of the liquid. More importantly, nonisothermal solidified phases in the joint were a preferential source of failure and crack propagation in tensile test. The intermetallic compounds were the source of mechanical weakness due to brittle cracking or delamination at the interface. For the base material with the FCC structure, the slip along the {111} planes was the dominant mechanism of deformation. Slip and plastic flow happened by shearing of certain crystallographic planes over one another. Slip occurred in a plane having the minimum inter atomic distance and planes having the greatest atomic density (Ref. 57). As it is shown in Table 6, the strength of the joints prepared with BVAg-18 is higher than both Cd-containing filler metals. As the X-ray analyses showed the presence of $CdCu_2$ (β_x), $CdCu_4$ (β_y), Ag_5Zn_8, CuZn (β'), and Cu_3Sn, Ag_3Sn phases between the substrate and interlayers play a crucial role in brazing strength of the joint. The existence of the intermetallic phases strongly deteriorates the brazing strength. It is also deduced that the brazing strength of the joint is strongly related to types of the interfacial reaction products. However, from a microstructural point of view, the change of joint strength with the brazing parameters was to a large extent dependent on the joint microstructure. When brazing was performed with BAg-1a and BAg-1 at 780°C for 2 min, the initial Ag in the interlayer reacted with Zn and Cd incompletely, leaving some residual Ag in the bond line after the brazing operation. During the

tensile test process, cracks easily occurred at the boundary of the intermetallic phases/residual Ag and the boundary of the intermetallic phases/Ag-based solid solution, subsequently expanded along the intermetallic phases and result in failure. On the other hand, when the brazing was performed with BVAg-18 at 780°C for 20 min Ag-based solid solution, intermetallic phases and Ag-Cu eutectic phases were mixed together in the bond line. This led to the highest joint strength. When the brazing temperature or time was increased, the bond line was mainly composed of the Ag-Cu-Sn intermetallics and Ag-Cu eutectic phase.

The optimum fatigue strength was achieved for joints prepared at 780°C for 20 min in vacuum using BVAg-18 filler metal. The test results for two atmospheres are shown in Fig. 19. The majority of specimens failed from surface sites remote from the bond line. The initiation sites were typically displaced from the bond line by approximately 0.8 mm or greater and almost equally divided between the parent material. It was seen that fatigue life of the copper-beryllium alloy brazed in argon is lower than that of those joined in vacuum. The fatigue test results also showed that when specimens were under low stress, fracture occurred on the corner of the joints. It is seen that cycling at ±12 MPa yield an average fatigue life of 7×10^5 cycles. At 18 Hz, it would take more than 34,000 h to accumulate the cycles. However, fatigue failure in the low-cycle and high-cycle regimes was often dominated by the crack initiation processes, which were strongly influenced by the salient features and brazing end products in the microstructure. Furthermore, both brittle and ductile fractures appeared in the joints — Fig. 20A, B. In the fracture surface, the conventional ductile fracture process generated the regions with dimples, whereas the faceted regions generated by an intergranular fracture mechanism. Initial cracks produced in the fine phase and expanded to other areas of the bond. The striations only appeared in higher magnification showing the dominant mechanism was not brittle fracture. The fatigue crack growth process involves damage accumulation and crack extension in the bond line. The fatigue striations develop because of the ability of dislocations to cross-slip and rearrange themselves into low energy cell structures in the saturated phase with Ag. From another standpoint, the large number of cycles required for crack growth allow a greater time for dislocation rearrangement into a cell configuration. This led to the formation of striation-like markings on the joints fracture surface due to an interaction between the crack front and the cell walls, with the spacing of the striation-like markings being equal to the spacing of the cell walls in the direction of crack propagation.

Conclusions

In this study, microstructural evolution of a copper-beryllium alloy was investigated when using different Ag-based interlayers. The important findings are as follows:

Partial transient liquid phase diffusion brazing of the copper-beryllium alloy has been successfully achieved using Ag-based filler metals. The interlayers reacted with the base metal resulting in the formation of $CdCu_2$ (β_x), $CdCu_4$ (β_y), Ag_5Zn_8, CuZn (β') and Cu_3Sn, Ag_3Sn, Ag-based solution, and Ag–Cu eutectic phases. The amount and morphology of all kinds of the reaction phases changed gradually with the brazing time and temperature.

Voids and porosities were observed within the joints prepared in argon atmosphere. Formations of these voids were related to the presence of argon impurities.

The micostructural studies revealed that the cross section of the interlayer decreased with increasing temperature and diffusion time. However, optimum hardness was achieved in both argon and vacuum at the higher brazing temperature.

The mutual effect of the brazing temperature and brazing time on the strength of the specimens showed different results in mechanical properties of the joints. Since the brazing time of the copper-beryllium alloy was dependent on the type and amount of the melting point depressants, the isothermal solidification time was dependent on the brazing temperature.

The relationship of the brazing parameters and joint strength was discussed, and the optimum brazing parameters were obtained. When brazed at 780°C for 20 min, the tensile strength was 156.8 MPa.

There was a critical brazing temperature to minimize the required time for isothermal solidification. Decreasing of isothermal solidification rate at brazing temperature of 780°C can be attributed to enrichment of residual liquid with some filler metal alloying elements particularly Sn and Cd, during dissolution and isothermal solidification.

Fatigue life of joints prepared at 780°C for 20 min in vacuum was more than those fabricated in argon atmosphere. In both low and high stresses, brittle and ductile fracture occurred. Fractography of the specimens showed that majority of cracks in the interface were intergranular.

Acknowledgment

The author would like to thank Dr. H. R. Madaah Hosseini and Prof. A. H. Kokabi from the Sharif University for helpful discussions and comments on the manuscript.

References

1. Hung, N. P., Zhong, Z. W., Lee, K. K., and Chai, C. F. 1999. Precision grinding and facing of copper-beryllium alloys. *J. Precision Engineering* 23(4): 293–304.

2. Bonfield, W., and Edwards, B. C. 1974. Precipitation hardening in Cu 1.81 wt. % Be 0.28 wt. % Co, Part 1 — Continuous precipitation. *Journal of Material Science* 9: 398–455.

3. Zalkind, S., and Moreno, D. 1999. Fracture characterization of welded copper–beryllium alloy. *J. Mater. Sci. Lett*. 18: 849–852.

4. Gale, W. F., and Wallach, E. R. 1991. Microstructural development in transient liquid phase bonding. *Metall. Trans.* A 22:2451–2457.

5. Bosco, N. S., and Zok, F. W. 2004. Critical interlayer thickness for transient liquid phase bonding in the Cu-Sn system. *Acta Mat.* 52, (10): 2965–2972.

6. Shirzadi, A. A., and Wallach, E. R. 1997. New approaches for transient liquid phase diffusion bonding of aluminum based metal matrix composites. *Mater. Sci. Technol.* 13: 135.

7. Atabaki, M. M. 2010. Recent progress in joining of ceramic powder metallurgy products to metals. *Metalurgija-Journal of Metallurgy* (MJoM) 16(4): 255–268.

8. Brochu, M., Pugh, M. D., and Drew, R. A. L. 2004. PTLPB of Si_3N_4 to FA-129 using nickel as a core interlayer. *International Journal of Refractory Metals and Hard Materials*, 22(2-3): 95–103.

9. Kin, J. J., Park, J.-W., and Eager, T. W. 2003. Interfacial microstructure of partial transient liquid phase bonded Si_3N_4-to-Inconel 718 joints. *Materials Science and Engineering* A, 344, 1–2 (3): 240–244.

10. Atabaki, M. M., and Hanzaei, A. T. 2010. Partial transient liquid phase diffusion bonding of Zircaloy-4 to stabilized austenitic stainless steel 321. *Materials Characterization* 61(10): 982–991.

11. Atabaki, M. M. 2010. Microstructural evolution in the partial transient liquid phase diffusion bonding of Zircaloy-4 to stainless steel 321 using active titanium filler metal. *Journal of Nuclear Materials* 406(3): 330–344.

12. Humpston, G., and Jacobson, D. M. 1994. *Principles of Soldering and Brazing.* ASM (8): 186–190.

13. Kinloch, A. J. 1987. *Adhesion and Adhesive-Science and Technology.* ASTM D1002-72 Standard test method for apparent shear strength of single-lap-joint adhesively bonded metal specimens by tension loading (Metal-to-Metal). pp. 195–200.

14. Kumar, S., and Pandey, P. C. 2011. Fatigue life prediction of adhesively bonded single lap joints. *International Journal of Adhesion and Adhesives* 31(1): 43–47.

15. Ebnesajjad, S. 2009. Testing of adhesive bonds. *Adhesives Technology Handbook*, second edition. pp. 273–287.

16. Bailey, G. L. J., and Watkins, H. C. 1951.

The flow of liquid metals on solid metal surfaces and its relation to soldering, brazing and hot dip coating. *J. Inst. Metals* 80: 57–76.

17. Klein, R. J. 1967. Wassink: Wetting of solid-metal surfaces by molten metals. *J. Inst. Metals*, 95, pp. 38–43.

18. Chen, S.-W., and Yen, Y.-W. 1999. Interfacial reactions in Ag-Sn/Cu couples. *Journal of Electronic Materials* 28(11): 1203–1208.

19. Bhadeshia, H. K. D. H. 2003. *Joining of Commercial Aluminium Alloys*, edited by S. Subramanian and D. H. Sastry. *Proceedings of International Conference on Aluminium INCAL 03*, Aluminium Association of India, Bangalore, p. 195.

20. Shewmon, P. G. 1989. *Diffusion in Solids*. Warrendale, Pa., The Metallurgical Society, 2nd ed., pp.19–25.

21. Yagmura, L., Duygulub, O., and Aydemir, B. 2011. Investigation of metastable γ' precipitate using HRTEM in aged Cu-Be Alloy, *Materials Science and Engineering*: A. Article in press, accepted manuscript, *doi:10.1016/j.msea.2011. 01.114*.

22. Williams, D. B., and Butler, E.P. 1981. Grain boundary discontinuous precipitation reactions. *Int. Metals Rev*. 26: 15.

23. Hirth, S., and Gottstein, G. 1998. Misorientation effects on discontinuous precipitation in Al-Ag-Ga. *Acta Mater*. 46(11): 3975–3984.

24. Wikstrom, N. P., Egbewande, A. T., and Ojo, O. A. 2008. High temperature diffusion induced liquid phase joining of a heat resistant alloy. *Journal of Alloys and Compounds*, 460, 1–2 (7): 379–385.

25. Lashko, N. F., and Lashko, S. V. 1977. Contact metallurgical processes in soldering metals. Moscow: Metallurgy Press.

26. Lee, K. H., Shin, M. C., and Lee, J. Y. 1986. A kinetic study of the silver-mercury contact reaction. *Journal of Materials Science* 21(7): 2430–2434.

27. Atabaki, M. M. 2011. Characterization of transient liquid-phase bonded joints in a copper-beryllium alloy with silver-base interlayer. *Journal of Materials Engineering and Performance*. *DOI: 10.1007/s11665-011-9953-9*.

28. Hill, A., and Wallach, E. R. 1989. Modelling solid-state diffusion bonding. *Acta Metal.* 37: 2425–2437.

29. Aksay, I. A., Hoge, C. E., and Pask, J. A. 1974. Wetting under chemical equilibrium and non-equilibrium conditions. *J. Phys. Chem.* 78(12): 1178–1183.

30. Lowell, J. M., and Chalmers, B. 1959. *Trans. TMS-AIME* 215: 499–506.

31. Okamoto, H. 2000. *Desk Handbook-Phase Alloys Diagrams for Binary Alloys*, second edition, ASM International.

32. Witusiewicz, V. T., Hecht, U., Rex, S., and Sommer, F. 2002. Partial and integral enthalpies of mixing of liquid Ag-Al-Cu and Ag-Cu-Zn alloys. *J. Alloys Compd*. 337: 189–201.

33. Drits, M. E., Bochvar, N. R., Guzei, L. S., Lysova, E. V., Padezhnova, E. M., Rokhlin, L. L., and Turkina, N. I. 1961. The Ag-Cd-Cu-Zn system (Silver-Cadmium-Copper-Zinc). *Journal of Phase Equilibria* 2(2): 228–230, *DOI: 10.1007/BF02881490.*

34. Li, J. F., Agyakwa, P. A., and Johnson, C. M. 2010. Kinetics of Ag_3Sn growth in Ag-Sn-Ag system during transient liquid phase soldering process. *Acta Materialia* 58(9): 3429–3443.

35. Belova, I. V., and Murch, G. E. 2001. The transition from Harrison type-B to type-A kinetics in grain-boundary tracer diffusion. *Philos. Mag.* 81: 2447.

36. Mei, Z., Sunwoo, A. J., and Morris, J. W. 1992. Analysis of low-temperature intermetallic growth in copper tin diffusion couples. *Metallurgical Transactions* A. 23S: 857–864.

37. Haimovich, J. 1993. Cu-Sn intermetallic compound growth in hot-air-levelled tin at and below 100°C. *AMP Journal of Technology* 3:46–54.

38. Tuah-Poku, I., Dollar, M., and Massalski, T. B. 1988. A study of the transient liquid phase bonding process applied to a Ag/Cu/Ag sandwich joint. *Metallurgical Transactions* A. 19A ,pp. 675–686.

39. Nakao, Y., Nishimoto, K., Shinzoki, K., and Kang, C. Y. 1989. Theoretical research on transient liquid insert metal diffusion bonding of nickel base alloys. *Trans. Jpn Weld. Soc*. 20, pp. 60–65.

40. Nakagawa, H., Lee, C. H., and North, T. H. 1991. Modelling of base metal transient liquid-phase brazing. *Metall. Trans* A. 22A:543–555.

41. Crank J., 1975. *The Mathematics of Diffusion*, second ed., Oxford University Press, Oxford, UK, p. 37.

42. Sinclair, C. W., Purdy, G. R., and Morral, J. E. 2000. Transient liquid-phase bonding in two-phase ternary systems. *Metall. Trans.* A. 31A: 1187–1192.

43. Zhou, Y., Gale, W. F., and North, T. H. 1995. Modelling of transient liquid phase diffusion bonding. Phase bonding. *Int Mater Rev.* 40(5): 181–96.

44. Gale, W. F., and Butts, D. A. 2004. Transient liquid phase bonding. *Sci Technol Wel Joining* 9(4): 283.

45. Zhou, Y., and North, T. H. 1994. Numerical model for the effect of grain boundaries on the total amount diffused. *Acta Metal Mater.* 42(3): 1025–1029.

46. MacDonald, W. D., and Eagar, T. W. 1998. Isothermal solidification kinetics of diffusion brazing. *Metall Mater Trans* A. 29A(1): 315–325.

47. Smith, C. S. 1948. Introduction to grains, phases, and interfaces-an interpretation of microstructure. *Trans. AIME* 175: 15–51.

48. Chatain, D., Rabkin, E., Derenne, J., and Bernardini, J. 2001. Role of the solid/liquid interface faceting in rapid penetration of a liquid phase along grain boundaries. *Acta Mater.* 49(7): 1123–1128.

49. Nam, H. S., and Srolovitz, D. J. 2007. Molecular dynamics simulation of Ga penetration along $\Sigma 5$ symmetric tilt grain boundaries in an Al bicrystal. *Phys. Rev.* B 76(18): 184114-1–184114-14.

50. Sigle, W., Richter, G., Ruhle, M., and Schmidt, S. 2006. Insight into the atomic-scale mechanism of liquid metal embrittlement. *Appl. Phys. Lett*. 89(12): 121911-1–121911-3. *doi:10.1063/1.2356322.*

51. Yin, L., and Sridhar, S. 2010. Effects of small additions of Tin on high-temperature oxidation of Fe-Cu-Sn alloys for surface hot shortness. *Metallurgical and Materials Transactions* B, 41B(10): 1095.

52. Kokawa, H., Lee, C. H., and North, T. H. 1991. Effect of grain boundaries on isothermal solidification during transient liquid phase brazing. *Metall Trans* A 22A: 1627–1631.

53. Saida, K., Zhou, Y., and North, T. H. 1993. The influence of base metal grain size on isothermal solidification during transient liquid-phase brazing of nickel. *J. Mater Sci.* 28: 6427–6432.

54. Ikeuchi, K., Zhou, Y., Kokawa, H., and North, T. H. 1992. Liquid-solid interface migration at grain boundary region during transient liquid phase brazing. *Metall Trans* A 23A(10): 2905–2915.

55. Atabaki, M. M., Hosseini, H. R. M., and Kokabi, A. H. 2009. Influence of the furnace brazing process parameters on the chemical heterogeneity, mechanical and physical properties of copper-beryllium alloy joints. *4th International Brazing & Soldering Conference*, Orlando, Fla.

56. Atabaki, M. M., and Idris, J. 2012. Low-temperature partial transient liquid phase diffusion bonding of Al/Mg_2Si metal matrix composite to AZ91D using Al-based interlayer. *Materials & Design* 34(1): 832-841.

57. Akbari Mousavi, S. A. A., and Niknejad, S. T. 2010. Study on the microstructure and mechanical properties of Nd:YAG pulsed laser beam weld of UNS-C17200 copper beryllium alloy. *Journal of Materials Processing Technology*, 210, 11, (8): 1472–1481.

AWS, Weld-Ed Web Site Promotes Welding Careers

The American Welding Society (AWS) and National Center for Welding Education & Training (Weld-Ed) Web site at *www.CareersInWelding.com* offers the following details: people and companies in the welding industry; fun facts; salary information; industry news; videos; articles; and upcoming training opportunities, seminars, and events.

Additionally, the site features pages geared directly for students with scholarship information and a welding school locator; for welding professionals to build a résumé, find welding-related jobs, and learn about AWS certifications; and for educators to discover tips for teachers and guidance counselors, information about curricula, professional development, and other resources.

This Web site serves a valuable tool for students, parents, educators, counselors, and welding professionals. It also allows visitors to send questions, comments, or ideas for people profiles.